oe-a

KFPE
Korea Flexible & Printed Electronics Society

PAPER • OPEN ACCESS

Aerosol jet printed temperature sensors using an environmentally friendly bilayer dielectric

View the article online for updates and enhancements.

Flexible and Printed Electronics

Aerosol jet printed temperature sensors using an environmentally friendly bilayer dielectric

Mathieu N Tousignant[1,5], Vanessa Tischler[1,5], Kaitlin Wagner[1], Zheng Sonia Lin[1,2], Jaclyn Brusso[2], Ricardo Izquierdo[3] and Benoît H Lessard[1,4,*]

1 Department of Chemical and Biological Engineering, University of Ottawa, 161 Louis Pasteur, Ottawa, ON, Canada
2 University of Ottawa, Department of Chemistry and Biomolecular Sciences, 10 Marie Curie, Ottawa, ON, Canada
3 École de Technologie Supérieure- Univesité du Québec, Department of Electrical Engineering, 1100 Notre-Dame Ouest, Montreal, QC, Canada
4 University of Ottawa, School of Electrical Engineering and Computer Science, 800 King Edward Ave., Ottawa, ON, Canada
5 Joint first author.
* Author to whom any correspondence should be addressed.

E-mail: benoit.lessard@uottawa.ca

Keywords: printed temperature sensors, bilayer dielectric, aerosol jet printing, bio-degradable materials, e-waste reduction

Supplementary material for this article is available online

Abstract

With the rise of the internet of things and applications such as smart packaging, the need for low cost, disposable temperature sensors with minimum environmental impact are critical. In this study, we report fully printed capacitive temperature sensors made from bio-degradable dielectric materials. All layers were aerosol jet printed and the areal capacitance was characterized at several temperatures between room temperature (22 °C) and 80 °C. Using a bilayer dielectric structure, a layer of poly (vinyl alcohol) (PVA) was encapsulated with polycaprolactone (PCL) through interfacial crosslinking to protect it against humidity. Various concentrations and layer amounts of PVA were investigated, with the most effective capacitors consisting of a single layer of PVA deposited from a 5.0 mg ml^{-1} solution followed by a layer of the UV-crosslink-able PCL deposited from 2.0 mg ml^{-1} solution, achieving a $43 \pm 6\%$ increase in areal capacitance at 80 °C when compared to room temperature, measured at a frequency of 501 Hz.

1. Introduction

The wearables and printed electronics industry has been growing steadily from its' value of less than 1 billion US dollars in 2009, with expectations to be worth 73.3 billion dollars by 2029 [1, 2]. Printed electronics enables low-cost mass production of electronics that are being implemented in a variety of short term sensing applications, e.g. onto disposable packaging [3]. These sensors can be used to monitor a product's temperature, humidity, or other conditions indicative in supply chain management [3, 4]. The growth of the printed electronics industry also causes an increase in e-waste, with an estimated 74.7 million metric tons of e-waste produced worldwide by 2030 [5]. To reduce the impact of e-waste, it is critical to select materials which have a reduced environmental impact at the devices' end-of-life. Given this, the chosen manufacturing and printing processes of new electronics is directly influenced by the properties of the

new materials and corresponding ink properties, and therefore a simple substitution of a new material often leads to significant changes in the printing parameters. Although there are many options for sustainable dielectrics[6], there are few examples of printed electronics sensors fabricated using sustainable materials [7, 8]. Efforts have been made to demonstrate the printability of such sustainable materials with several printing methods allowing for direct writing for quick and simple customization [6, 9–15]. These printing techniques deposit the ink in a controlled area on the substrate which can reduce waste and enable printing on complex 3D surfaces [16–18]. As a result, the choice of process will also depend on the throughput, device area and complexity of the print, which may require techniques such as inkjet and aerosol jet over blade coating and roll to roll printing [9–11]. Inkjet and aerosol jet are non-contact techniques, providing better freedom of movement and adaption to irregular or 3D surfaces. In order to successfully
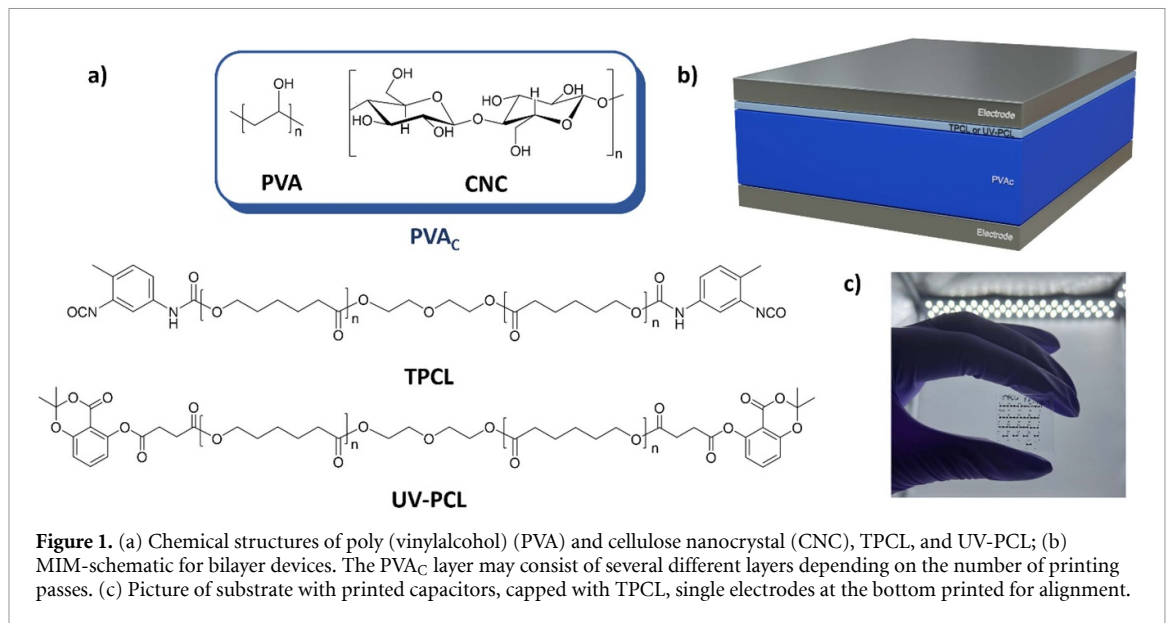
Figure 1. (a) Chemical structures of poly (vinylalcohol) (PVA) and cellulose nanocrystal (CNC), TPCL, and UV-PCL; (b) MIM-schematic for bilayer devices. The PVA_C layer may consist of several different layers depending on the number of printing passes. (c) Picture of substrate with printed capacitors, capped with TPCL, single electrodes at the bottom printed for alignment.

print on such surfaces or with complex materials, a curing step can be incorporated, which is often termed 4D-printing [15, 19]. Inkjet printing typically requires low viscosity inks whereas aerosol jet printing is amenable to a larger range of viscosities [11]. Furthermore, while inkjet printing is often successful, aerosol jet has a larger working distance, ensuring more distance to the target, and the atomization of the functional inks that can inherently suppress surface tension effects which may lead to poor patterning [13, 14, 20].

One way to fill this gap within the smart packaging industry is to improve the mechanical and electrical properties of commercially available sustainable materials [21]. We recently reported improved dielectric materials with negligible moisture sensitivity using bilayers of poly (vinyl alcohol) (PVA) and polycaprolactone (PCL) [22, 23]. Both materials are compostable and currently produced on the ton scale, making them good candidates to be quickly adopted into printed electronics manufacturing [24, 25]. The PCL polymer was functionalized with either toluene diisocyanate (TPCL) end groups or benzodioxinone (UV-PCL) end groups, enabling thermal or UV-crosslinking with the hydroxy groups of PVA at the PVA/PCL interface. PVA has been reported to exhibit changes in electrical properties when exposed to changes in temperature [26]. However, PVA is well known to be hygroscopic and has previously been applied as a humidity sensor [27–30]. Including a thin PCL coating (figure 1) with interfacial crosslinking creates a barrier to moisture improving the stability of PVA and allows for further orthogonal processing, which is essential to decouple the temperature and humidity response [23, 31]. For example, when fabricating thin-film transistors (TFTs) with a PVA dielectric, an increase in temperature will increase device hysteresis which is due to a change

in the frequency dependant capacitance of PVA [26, 32, 33]. This is caused by the PVA softening with an increase in temperature which facilitates the alignment of space charges present due to imperfections and the hydroxy groups with the applied electric field increasing the capacitance [26, 34, 35].

In this work, a PVA/cellulose nanocrystal blend (PVA_C) was used as the high-*k* dielectric material ($k \sim 12$)[23] while either TPCL or UV-PCL as a low-*k* ($k \sim 4$) [23, 31] dielectric material to create high-*k*/low-*k* bilayer dielectrics. Metal-insulator-metal (MIM) capacitors were fabricated on glass substrates using aerosol jet printing. A silver nanoparticle ink was used to print the top and bottom electrodes. These devices were characterized at various temperatures to analyze their change in capacitance vs temperature. Three different MIM capacitors configurations were investigated: PVA_C, PVA_C/TPCL and PVA_C/UV-PCL and in all cases an increase in capacitance was measured in response to an increase in temperature from 22°C to 80 °C. These findings demonstrate that fully printed temperature sensors can be fabricated using a low cost environmentally friendly bilayer dielectric system.

2. Experimental

2.1. Materials

The silver electrodes were printed using a Novacent Metalon JS-A221AE silver nanoparticle ink with 50 wt% loading. PVA $M_w = 31\,000$–$50\,000$ Da; 98%–99% hydrolyzed, PCL diol ($M_w = 2000$ Da) and toluene-2,4-diisocyante (95%) and were purchased through Sigma-Aldrich. TPCL and UV-PCL were synthesized following previously reported procedures [31]. The PVA was dissolved in distilled water with 0.75 wt% CNCs dispersed in the solutions at PVA concentrations of 5.0 and 10.0 mg ml^{-1}. The TPCL

and UV-PCL were dissolved in anhydrous toluene at concentrations of 2.0 mg ml^{-1}.

2.2. Printing

An Optomec Aerosol Jet FLEX (AJ5X) printer was used to fabricate the MIM capacitors. The PVA$_C$ was printed at concentrations of 5 and 10 mg ml^{-1} with the following settings. Nozzle size: 300 μm, plate temperature: 25 °C, sheath: 100 ccm, atomizer power: 45 V, atomizer: 40 ccm and speeds of 2 mm s^{-1}. TPCL and UV-CPL were printed at 2.0 mg ml^{-1} with the following settings: nozzle: 300 μm, plate temperature: 25 °C, sheath: 150 ccm, atomizer power: 23 V, atomizer: 40 ccm and speeds of 2 mm s^{-1}. The silver nanoparticle ink was printed with the following settings. Sheath: 100 ccm, atomizer power: 45 V, atomizer: 45 ccm and speeds of 2 mm s^{-1}. The top silver electrode was printed over twice to avoid having any breaks between the top electrode and the contact pads due to the height of the dielectric layer.

2.3. Optical profilometry

2D and 3D profilometry scans were completed using a cyberTECHNOLOGIES CT100 optical profilometer (cyberTECHNOLOGIES GmbH) and Golden Surfer® 11 Software to visualize the surface and side profiles for the 3D imaging.

2.4. Electrical characterization

The capacitors were tested using a PGSTAT204 potentiostat from Metrohm Autolab connected with two electrical probes to contact the capacitor electrodes with, placed inside a Faraday cage. Using the Nova 2.1.3 software from Metrohm Autolab for control, the real as well as imaginary parts of the impedance Z together with their phase angle δ were measured at 10 different frequencies per decade (logarithmically spaced out), between 1 MHz and 0.1 Hz. However, below 100 Hz the measurements became exceedingly noisy, leaving an effective range of 1 MHz to 100 Hz. In potentiostatic measurements, the frequency dependant capacitance is calculated from the real and imaginary portions of the impedance, Z' and Z'' respectively, using the following equation [36]

$$C = \frac{1}{2\pi f}\left(\frac{Z''}{Z''^2 + Z'^2}\right).\tag{1}$$

After letting the substrates reach the specific temperature on an RCT basic hotplate from IKA for at least 10 min, the testing was repeated for each working device at 40 °C, 50 °C, 60 °C, 70 °C, and 80 °C.

3. Results and discussion

3.1. Microscope imaging

The capacitance scales inversely with material thickness, where the total capacitance of multilayered materials is characterized by equation (2). Therefore,

the lowest capacitance will have a large impact on the total capacitance of the dielectric system [37, 38],

$$\frac{1}{C_{\text{tot}}} = \frac{1}{C_1} + \frac{1}{C_2} + \frac{1}{C_3} + \dots .\tag{2}$$

It is challenging to print uniform thin layers (<100 nm) by aerosol jet printing and as such, it is difficult to fabricate bilayer dielectrics without the appearance of defects, such as pinholes. However, in our previous paper, we showed it to be possible to deposit a thick layer of TPCL or UV-PCL, which when crosslinked to the PVA interface and subsequently rinsed with toluene to remove any excess PCL, led to a very thin layer of TPCL or UV-PCL on the PVA$_C$ [23, 31]. This strategy enables the fabrication of a pin-hole free thin low-k layer by forming a monolayer and preventing pooling and delamination. To demonstrate this, figure 2 shows microscope images of aerosol jet printed PVA$_C$ with a TPCL or UV-PCL top layer, before and after toluene rinsing for 10 s. The TPCL was thermally crosslinked, and the UV-PCL was crosslinked under UV light prior to imaging. Figure 2 shows that the excess PCL can be removed with a simple rinsing step leaving behind a thin layer of PCL on top of the PVA$_C$.

3.2. Layer thickness comparison

The primary goal of this study was to demonstrate a fully printed PVA/PCL bilayer capacitor system, and as such various printing techniques were considered and investigated. Initial depositions demonstrated that blade coating PVA from a water-based solution caused the films to dry unevenly on the silver electrodes due to poor surface adhesion as well as the low volatility of water. We explored a variety of solvent additives, blade geometries and processing conditions with little reproducible success. Furthermore, the dewetting challenges could not be rectified by employing other deposition techniques such as spray-coating or slot-die coating (see figure S1). Alternatively, aerosol jet printing showed promise to circumvent the PVA film forming challenges. Aerosol jet printing atomizes the polymer solution enabling it to quickly dry on the substrate and reduce the coffee ring effect seen with other techniques that have slower drying times [12]. The use of aerosol jet printing has been previously demonstrated for depositing dielectric materials for both capacitor and TFTs [11, 39–44]. Several of these studies have highlighted the usefulness of aerosol jet printing for PVA specifically, as the dielectric material [39, 41, 42]. Therefore, we employed aerosol jet printing for the fabrication of our fully printed bilayer dielectric based temperature sensors.

As detailed in the Experimental section, the silver electrode was first printed, followed by the printing of PVA$_C$, then either TPCL or UV-PCL followed by another silver electrode. After the deposition of the TPCL or UV-PCL, interfacial crosslinking was
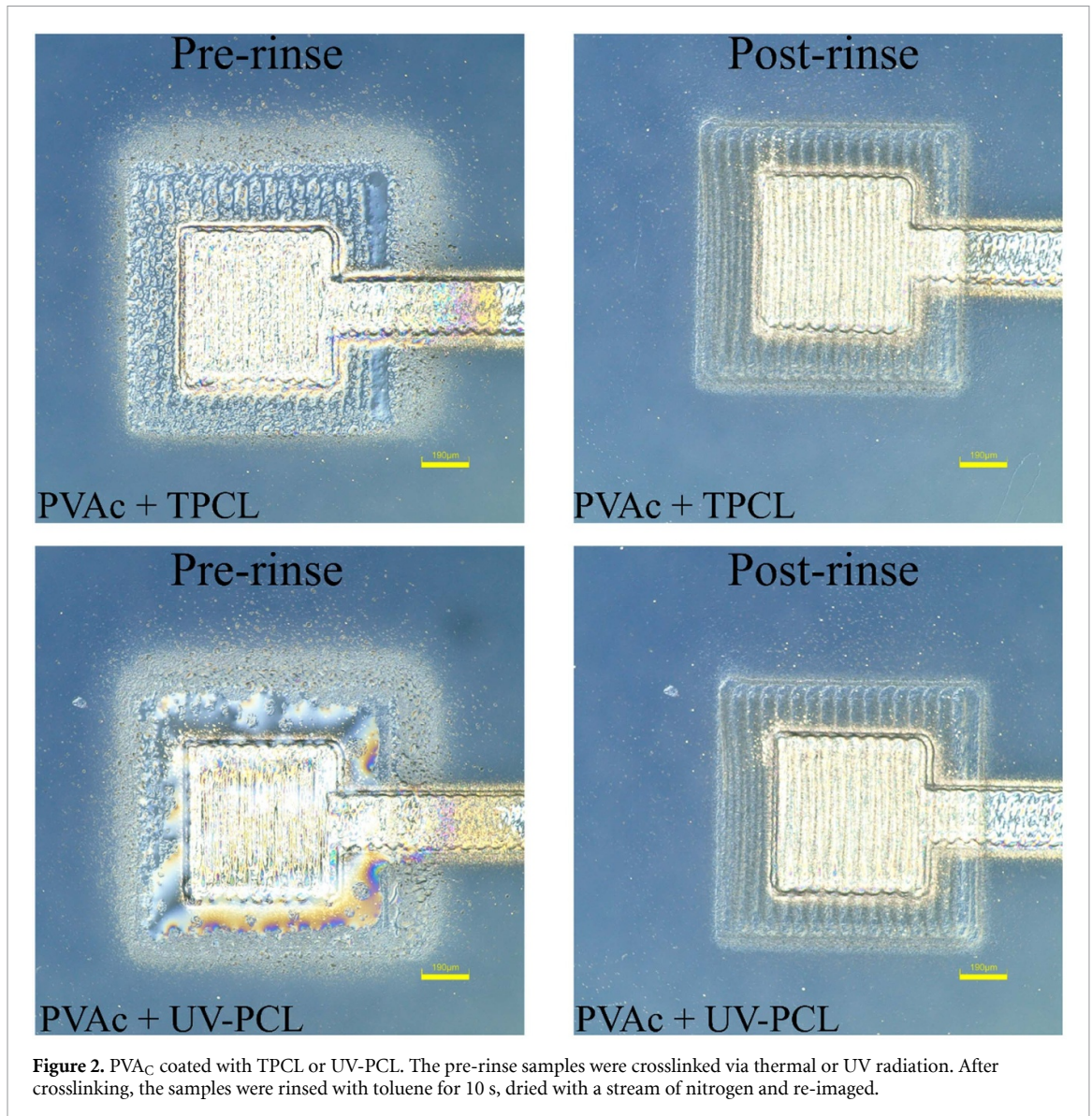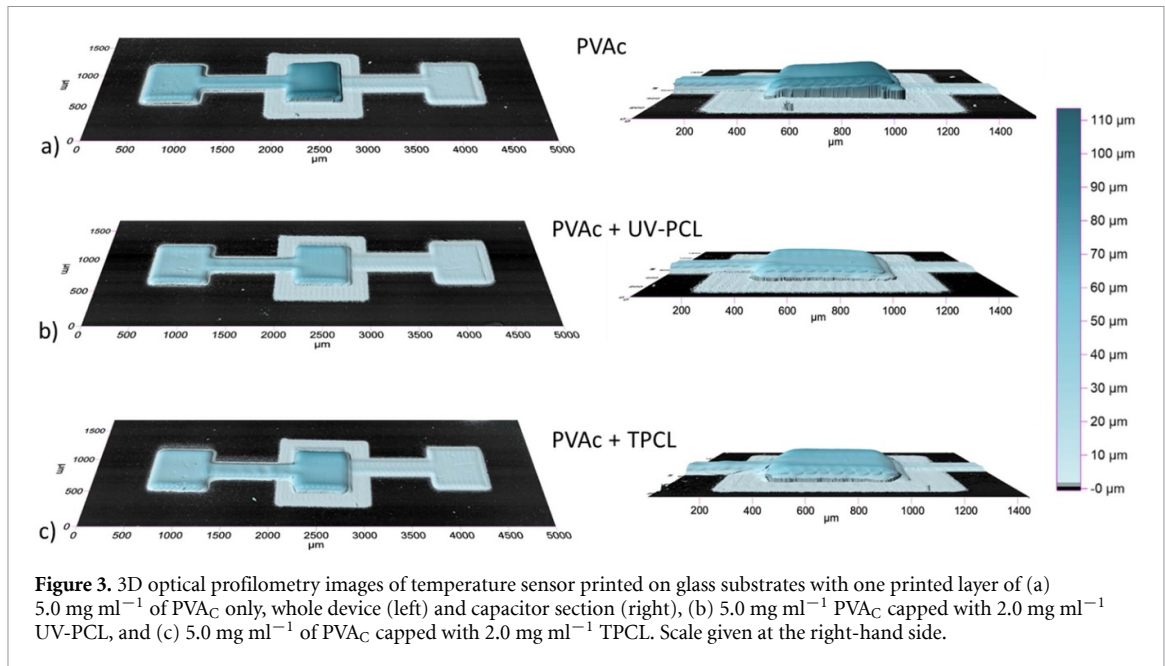
Figure 2. PVA$_C$ coated with TPCL or UV-PCL. The pre-rinse samples were crosslinked via thermal or UV radiation. After crosslinking, the samples were rinsed with toluene for 10 s, dried with a stream of nitrogen and re-imaged.

activated by either heat or UV-light prior to the final electrode deposition [23, 31]. Figure 3 highlights 3D optical profilometry scans of the sensors fabricated with the PVA$_C$ with UV-PCL or TPCL (2.0 mg ml^{-1}) bilayer compared to bare PVA$_C$ as a baseline to analyze the effectiveness of the PCL layer on preventing moisture contamination. After having been characterized and stored in ambient air for five days, it is evident that when only using PVA$_C$ with no PCL, the overall height of the device is greater (120 μm) than when coating the PVA$_C$ with TPCL (82 μm) or with UV-PCL (78 μm). This observation is reproducible and is consistent with PVA swelling with the absorption of moisture [31], demonstrating that the PCL provides a successful moisture barrier for the PVA.

In attempts to optimize device fabrication and the resulting performance, we explored different solution concentrations as well as depositing multiple PVA$_C$ layers to increase the overall dielectric thickness. Tables 1 and S1 summarize the film optimization through characterization of average height, maximum height, average roughness, and root-mean-square (RMS) roughness of the polymer layer. Measurements were taken along the polymer edge adjacent to the center of the device, as shown in figure S2. When using a 5.0 mg ml^{-1} of PVA$_C$, an additional layer (2 deposition of the same solution) was measured to have roughly doubled the height for both uncapped devices and those capped with UV-PCL (table 1). A slight increase in the roughness of the corresponding films made from 5.0 mg ml^{-1} was also measured with the addition of a second layer. The devices capped with TPCL measured a smaller increase in height of approximately 2 μm with the additional layer of PVA$_C$, compared to the other devices, whose overall thickness

Figure 3. 3D optical profilometry images of temperature sensor printed on glass substrates with one printed layer of (a) 5.0 mg ml^{-1} of PVA$_C$ only, whole device (left) and capacitor section (right), (b) 5.0 mg ml^{-1} PVA$_C$ capped with 2.0 mg ml^{-1} UV-PCL, and (c) 5.0 mg ml^{-1} of PVA$_C$ capped with 2.0 mg ml^{-1} TPCL. Scale given at the right-hand side.

Table 1. Summary of 2D optical profilometry scans for devices containing increasing layers of 5.0 mg ml^{-1} PVA$_C$ and those capped with 2.0 mg ml^{-1} of UV-PCL and TPCL; including the maximum change in areal capacitance.

Exp. conditions [a] with # layers		H_{AVE} [b] (mm)	H_{MAX} [b] (mm)	R_{AVE} [b] (mm)	R_{RMS} [b] (mm)	ΔC_0 [c] (%)
1 × PVA$_C$		2.95 ± 0.39	4.60 ± 0.54	0.36 ± 0.06	0.46 ± 0.08	36 ± 2
2 × PVA$_C$		6.35 ± 0.19	8.26 ± 0.26	0.41 ± 0.07	0.51 ± 0.07	44 ± 7
1 × PVA$_C$	1 × UV-PCL	2.90 ± 0.12	4.78 ± 0.54	0.48 ± 0.06	0.56 ± 0.07	43 ± 6
2 × PVA$_C$		6.09 ± 0.63	8.26 ± 0.46	0.56 ± 0.07	0.68 ± 0.09	38 ± 3
1 × PVA$_C$	1 × TPCL	3.02 ± 0.31	4.49 ± 0.32	0.28 ± 0.03	0.36 ± 0.04	36 ± 2
2 × PVA$_C$		4.99 ± 0.79	7.15 ± 1.01	0.44 ± 0.12	0.54 ± 0.13	44 ± 7

[a] PVA$_C$ layer was deposited using 5.0 mg ml^{-1} solution in distilled water. UV-PCL and TPCL layers were deposited using 2.0 mg ml^{-1} solution in anhydrous toluene. # of Layers refers to the deposition passes of the PVA$_C$ solution prior to UV-PCL or TPCL.

[b] H_{AVE} and H_{MAX} are the average and max height (thickness) of the film and R_{AVE} and R_{RMS} are the average roughness and RMS roughness respectively.

[c] ΔC_0 is the relative percent (%) change in areal capacitance between room temperature and 80 °C taken at 501 Hz.

increased by 3 μm. Upon increasing the PVA$_C$ concentration to 10.0 mg ml^{-1}, single-layer films exhibited a similar initial thickness, and slightly thicker secondary layers of 3.80 and 4.04 μm for the UV-PCL and TPCL layers respectively (table S1). The first layer of devices capped with UV-PCL was notably thinner, leading to overall thinner stack which could account for the variation in measured average roughness and RMS roughness compared to bare PVA$_C$ and PVA$_C$/TPCL. Overall, these results demonstrate that PVA$_C$/UV-PCL and PVA$_C$/TPCL bilayers can be successfully printed using aerosol jet printing, where roughness and thickness can be easily controlled through sequential depositions, and choice of solution concentration does not affect the print quality.

3.3. Capacitor

The capacitors were characterized by their areal capacitance C_0 rather than their relative permittivity k.

The best performing devices were obtained using a single layer of 5.0 mg ml^{-1} PVA$_C$ capped with 2.0 mg ml^{-1} TPCL, and their electrical characterization is shown in figure 4. All other devices and conditions are found in the supporting information (tables S2 and S3). Figure 4(a) demonstrates the consistent change in C_0 as a function of operating frequency and temperature. A minimum of four devices were printed for every condition, and with a total measured area of 0.39 ± 0.02 mm^2, averaged together led to significant error bars. The relative change of the C_0 of each device was calculated using the following equation:

$$\Delta C_0 = \left(\frac{C_{0T} - C_{0RT}}{C_{0RT}} \right) * 100\% \qquad (3)$$

with C_{0RT} being the areal capacitance at room temperature, and C_{0T} the areal capacitance at the specific temperature. We note that we consistently observed
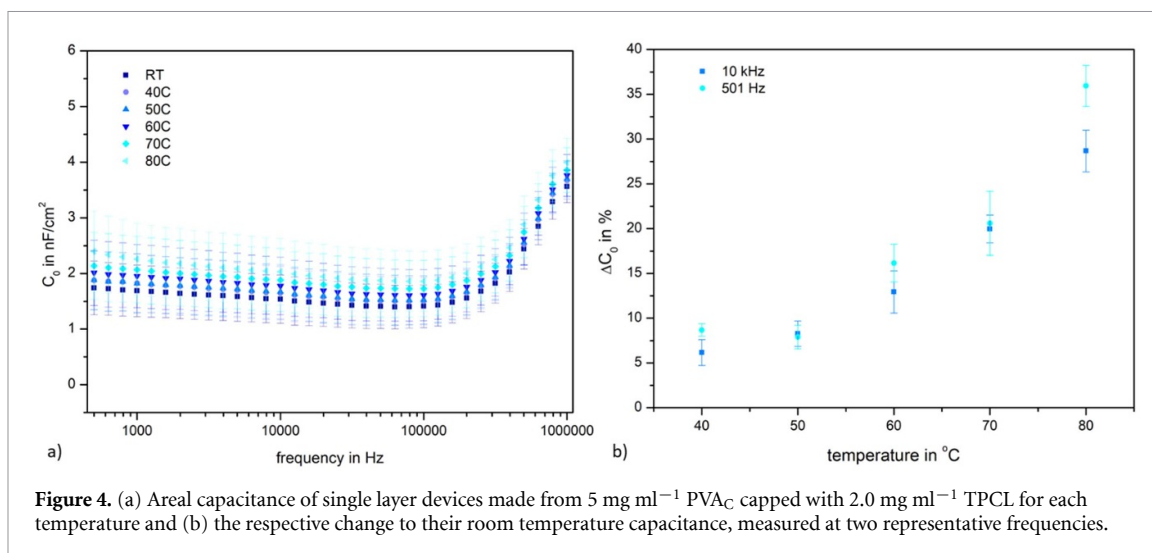
Figure 4. (a) Areal capacitance of single layer devices made from 5 mg ml^{-1} PVA$_C$ capped with 2.0 mg ml^{-1} TPCL for each temperature and (b) the respective change to their room temperature capacitance, measured at two representative frequencies.

an increase in C_0 for all devices above 1 MHz, regardless of the polymer thickness or amount of layers and therefore it is a result of the device architecture, electrode selection and/or operating conditions. We believe this increase is due to the transition between capacitive region to inductive region where parasitic inductance becomes more significant and we begin to observe electrode skin effects, proximity effects and dielectric loss effects, which can all increase the capacitance at high frequency. These results further demonstrate the importance of operating conditions, such as frequency, when characterizing capacitors. As can be seen in figure 4(b), the ΔC_0 with temperature was statistically significant for each device, with a greater increase in ΔC_0 at lower frequencies upon temperature increase compared to higher frequencies. At the lowest reliable frequency of 501 Hz, which consistently gave percentual changes in capacitance larger than the measured noise, ΔC_0 increased by 36% $\pm$ 2% at 80 °C compared to room temperature, while it was only an increase of 11% $\pm$ 3% at the highest reliable frequency of 1.0 MHz (figure S4).

Further characterization of devices fabricated using uncapped 5.0 mg ml^{-1} PVA$_C$ is summarized in figure S4, while the remaining characterization of devices capped with TPCL and UV-PCL are found in figures S5 and S6, respectively. A summary of calculated ΔC_0 values at 40 °C and 80 °C can be found in table S2. Devices made from one and two layers of 5.0 mg ml^{-1} PVA$_C$, uncapped and capped with TPCL showed similar electrical responses to those capped with UV-PCL, however their response had greater variability (error bars) at lower temperatures. Furthermore, we found that for devices printed from 5.0 mg ml^{-1} PVA$_C$ an increase in height also slightly increased the performance in uncapped capacitors and those capped with TPCL, as summarized in table 1. However, devices with 5.0 mg ml^{-1} PVA$_C$ capped with UV-PCL output a higher signal for thinner devices, with bilayers having a $\Delta C_0 = 38 \pm 3\%$ at

80 °C and 501 Hz, while single layer devices showed a $\Delta C_0 = 43 \pm 6\%$. At higher frequencies, the areal capacitance for the single layer device was lower with only 3.6 $\pm$ 0.7% when measured at 1.0 MHz.

Optimal devices were obtained using a single or double layer of PVA$_C$ capped with TPCL or UV-PCL. An improvement in signal was often reported when going from a single to a double layer of PVAc as the film thickness increased. When increasing to a third layer we observed a significant increase in the error associated to the uneven film formation and thickness variation, leading to unreliable devices, as demonstrated to figures S6 and S7.

4. Conclusion

We present fully printed capacitive temperature sensors that contain sustainably driven biodegradable polymers as dielectric materials. It was shown that single layer and multi-layer devices at varying concentrations could be successfully fabricated with aerosol jet printing, resulting in uniform layers with no excessive change in surface roughness of the devices. The percentual change of ΔC_0 increased consistently with temperature, with the low variability were measured at frequencies around 500 Hz to ensure the strongest ΔC_0 response. For single PVA$_C$ layer devices printed from 5.0 mg ml^{-1} PVA$_C$, capping with UV-PCL not only provided protection against ambient humidity for the PVA$_C$ but also gave the strongest ΔC_0 of 43 $\pm$ 6% at 80 °C. For devices with two layers of PVA$_C$, capping with TPCL yielded the best capacitors with ΔC_0 of 44 $\pm$ 7% at 80 °C.

Data availability statement

All data that support the findings of this study are included within the article (and any supplementary files).

Acknowledgments

ORCID iD

Benoît H Lessard ⬤ https://orcid.org/0000-0002-9863-7039

References

[1] Khan Y, Thielens A, Muin S, Ting J, Baumbauer C and Arias A C 2020 A new frontier of printed electronics: flexible hybrid electronics *Adv. Mater.* **32** 1–29

[2] Leenen M A M, Arning V, Thiem H, Steiger J and Anselmann R 2009 Printable electronics: flexibilty for the future *Phys. Status Solidi* a **206** 588–97

[3] Fattori M *et al* 2020 A fully-printed organic smart temperature sensor for cold chain monitoring applications *2020 IEEE Custom Integrated Circuits Conf. (CICC)* vol 2020 (IEEE) pp 1–4

[4] Chen S, Brahma S, Mackay J, Cao C and Aliakbarian B 2020 The role of smart packaging system in food supply chain *J. Food Sci.* **85** 517–25

[5] Rajesh R, Kanakadhurga D and Prabaharan N 2022 Electronic waste: a critical assessment on the unimaginable growing pollutant, legislations and environmental impacts *Environ. Chall.* **7** 100507

[6] Sanchez-Duenas L, Gomez E, Larrañaga M, Blanco M, Goitandia A M, Aranzabe E and Vilas-Vilela J L 2023 A review on sustainable inks for printed electronics: materials for conductive, dielectric and piezoelectric sustainable inks *Materials* **16** 3940

[7] Camus A, Reali M and Santato C 2022 Advances in high-resolution printed transistors: the case of bio-sourced organic materials *Curr. Opin. Green Sustain. Chem.* **34** 100594

[8] Oliveira J, Correia V, Castro H, Martins P and Lanceros-Mendez S 2018 Polymer-based smart materials by printing technologies: improving application and integration *Addit. Manuf.* **21** 269–83

[9] Grau G and Subramanian V 2020 Dimensional scaling of high-speed printed organic transistors enabling high-frequency operation *Flex. Print. Electron.* **5** 014013

[10] Chung S, Cho K and Lee T 2019 Recent progress in inkjet-printed thin-film transistors *Adv. Sci.* **6** 1801445

[11] Wiklund J *et al* 2021 A review on printed electronics: fabrication methods, inks, substrates, applications and environmental impacts *J. Manuf. Mater. Process.* **5** 89

[12] Carlos E, Branquinho R, Martins R and Fortunato E 2021 New challenges of printed high-κ oxide dielectrics *Solid-State Electron.* **183** 108044

[13] Gamba L, Johnson Z T, Atterberg J, Diaz-Arauzo S, Downing J R, Claussen J C, Hersam M C and Secor E B 2023 Systematic design of a graphene ink formulation for aerosol jet printing *ACS Appl. Mater. Interfaces* **15** 3325–35

[14] Secor E B 2018 Principles of aerosol jet printing *Flex. Print. Electron.* **3** 035002

[15] Areias C, Piro Y, Ranasingha O and Akyurtlu A 2023 A new techniue for 3D printing dieletric structures using aerosol-jettable photopolymers *Flex. Print. Electron.* **8** 015009

[16] Zhu Z, Ng D W H, Park H S and McAlpine M C 2020 3D-printed multifunctional materials enabled by artificial-intelligence-assisted fabrication technologies *Nat. Rev. Mater.* **6** 27–47

[17] Lee J, Kim H C, Choi J W and Lee I H 2017 A review on 3D printed smart devices for 4D printing *Int. J. Precis. Eng. Manuf.—Green Technol.* **4** 373–83

[18] 2016 *Organic and Printed Electronics—Fundamentals and Applications* (Pan Stanford Publishing Pte. Ltd.)

[19] Ranasingha O K, Haghzadeh M, Sobkowicz M J, Kingsley E, Armiento C and Akyurtlu A 2021 Formulation and characterization of sinterless barium strontium titanate (BST) dielectric nanoparticle ink for printed RF and microwave applications *J. Electron. Mater.* **50** 3241–8

[20] Degryse O, Bloemen V and Ferraris E 2022 Collagen composite inks for Aerosol Jet (R) printing in bone tissue engineering applications *Proc. CIRP* **110** 180–5

[21] Tan M J *et al* 2016 Biodegradable electronics: cornerstone for sustainable electronics and transient applications *J. Mater. Chem.* C **4** 5531–58

[22] Tousignant M N, Rice N A, Peltekoff A, Sundaresan C, Miao C, Hamad W Y and Lessard B H 2020 Improving thin-film properties of poly (vinyl alcohol) by the addition of low-weight percentages of cellulose nanocrystals *Langmuir* **36** 3550–7

[23] Tousignant M N, Rice N A, Niskanen J, Richard C M, Ritaine D, Adronov A and Lessard B H 2021 High performance organic electronic devices based on a green hybrid dielectric *Adv. Electron. Mater.* **7** 2100700

[24] De Prisco N, Immirzi B, Malinconico M, Mormile P, Petti L and Gatta G 2002 Preparation, physico-chemical characterization, and optical analysis of polyvinyl alcohol-based films suitable for protected cultivation *J. Appl. Polym. Sci.* **86** 622–32

[25] Liu K, Tran H, Feig V R and Bao Z 2020 Biodegradable and stretchable polymeric materials for transient electronic devices *MRS Bull.* **45** 96–102

[26] Subbarao N V V, Mandal S, Gedda M, Iyer P K and Goswami D K 2018 Effect of temperature on hysteresis of dipolar dielectric layer based organic field-effect transistors: a temperature sensing mechanism *Sens. Actuators* **269** 491–9

[27] Amin E M, Karmakar N C and Winther-Jensen B 2013 Polyvinyl-alcohol (PVA)-based RF humidity sensor in microwave frequency *Prog. Electromagn. Res.* B **54** 149–66

[28] Bergo P, Moraes I C F and Sobral P J A 2012 Effects of different moisture contents on physical properties of PVA-gelatin films *Food Biophys.* **7** 354–61

[29] Lu D *et al* 2014 Humidity dependent permittivity characterization of polyvinyl-alcohol film and its application in relative humidity RF sensor *European Microwave Week 2014 Connect. Future EuMW 2014—Conf. Proc. EuMC 2014 44th European Microwave Conf.* pp 163–6

[30] Subbarao N V V, Gedda M, Iyer P K and Goswami D K 2016 Organic field-effect transistors as high performance humidity sensors with rapid response, recovery time and remarkable ambient stability *Org. Electron.* **32** 169–78

[31] Tousignant M N, Lin Z S, Brusso J and Lessard B H 2023 Interfacial ultraviolet cross-linking of green bilayer dielectrics *ACS Appl. Mater. Interfaces* **15** 3680–8

[32] Egginger M, Irimia-Vladu M, Schwödiauer R, Tanda A, Frischauf I, Bauer S and Sariciftci N 2008 Mobile ionic impurities in poly (vinyl alcohol) gate dielectric: possible source of the hysteresis in organic field-effect transistors *Adv. Mater.* **20** 1018–22

[33] Wang W, Ma D, Pan S and Yang Y 2012 Hysteresis mechanism in low-voltage and high mobility pentacene thin-film transistors with polyvinyl alcohol dielectric *Appl. Phys. Lett.* **101** 033303

[34] Shekar B C, Veeravazhuthi V, Sakthivel S, Mangalaraj D and Narayandass S K 1999 Growth, sturcture, dielectric and AC conduction properties of solution grown PVA films *Thin Sold Films* **348** 122–9

[35] Reddy C, S. V, Han X, Zhu Q-Y, Mai L-Q and Chen W 2006 Dielectric spectroscopy studies on (PVP + PVA) polyblend film *Microelectron. Eng.* **83** 281–5

[36] Joshi J H, Kanchan D K, Joshi M J, Jethva H O and Parikh K D 2017 Dielectric relaxation, complex impedance and modulus spectroscopic studies of mix phase rod like cobalt sulfide nanoparticles *Mater. Res. Bull.* **93** 63–73

[37] Halliday D, Resnick R and Walker J 2007 *Physik Bachelor-Edition* (WILEY-VCH Verlag GmbH & Co. KGaA)

[38] *Dictionary of Electronics and Electrical Engineering* 2018 (Oxford University Press)

[39] Gupta A A, Bolduc A, Cloutier S G and Izquierdo R 2016 Aerosol jet printing for printed electronics rapid prototyping *2016 IEEE Int. Symp. on Circuits and Systems (ISCAS)* (IEEE) pp 866–9

[40] Gupta A A, Rahmani M H, Soer M C M, Cloutier S G and Izquierdo R 2020 Aerosol jet printed, microwave microstrip ring resonators for system-in-package applications *IEEE Trans. Compon. Packag. Manuf. Technol.* **10** 1913–20

[41] Monne M A, Howlader C Q, Mishra B and Chen M Y 2021 Synthesis of printable polyvinyl alcohol for aerosol jet and inkjet printing technology *Micromachines* **12** 220

[42] Mishra B, Howlader C Q and Chen M 2022 Completely printed flexible carbon nanotube based transistor using poly-vinyl alcohol (PVA) as gate dielectric via aerosol jet printing *Proc. SPIE* **12211** 1221101

[43] Ha M, Seo J-W T, Prabhumirashi P L, Zhang W, Geier M L, Renn M J, Kim C H, Hersam M C and Frisbie C D 2013 Aerosol jet printed, low voltage, electrolyte gated carbon nanotube ring oscillators with sub-5 μs stage delays *Nano Lett.* **13** 954–60

[44] Kim S H, Hong K, Lee K H and Frisbie C D 2013 Performance and stability of aerosol-jet-printed electrolyte-gated transistors based on poly(3-hexylthiophene) *ACS Appl. Mater. Interfaces* **5** 6580–5